Title: Ventilation versus biology: What is the controlling mechanism of nitrous oxide distribution in the North Atlantic?

Authors:

Mercedes de la Paz[1], Maribel I. García-Ibáñez[1], Reiner Steinfeldt[2], Aida F. Ríos[1†], Fiz F. Pérez [1]

[1]Instituto de Investigaciones Marinas (IIM-CSIC), Eduardo Cabello 6, 36208 Vigo, Spain.

[2] Institute of Environmental Physics, University of Bremen, Bremen, Germany
[†]Deceased

Corresponding author: Mercedes de la Paz (mercedes.delapaz@iim.csic.es)

Key points:

- We combined N_2O measurements and water mass mixing model in the North Atlantic
- Mixing of water masses and basin scale remineralization explain 72% of the N_2O distribution in the North Atlantic
- Preformed O_2 content and water mixing have an overlooked impact in the N_2O:O_2 ratio

This article has been accepted for publication and undergone full peer review but has not been through the copyediting, typesetting, pagination and proofreading process which may lead to differences between this version and the Version of Record. Please cite this article as doi: 10.1002/2016GB005507

Abstract

The extent to which water mass mixing and ocean ventilation contribute to nitrous oxide (N_2O) distribution at the scale of oceanic basins is poorly constrained. We used novel N_2O and chlorofluorocarbon (CFC) measurements along with multiparameter water mass analysis to evaluate the impact of water mass mixing and Atlantic meridional overturning circulation (AMOC) on N_2O distribution along the OVIDE section, extending from Portugal to Greenland. The biological N_2O production has a stronger impact on the observed N_2O concentrations in the water masses travelling northwards in the upper limb of the AMOC than those in recently ventilated cold water masses in the lower limb, where N_2O concentrations reflect the colder temperatures. The high N_2O tongue, with concentrations as high as 16 nmol kg^{-1}, propagates above the isopycnal surface delimiting the upper and lower AMOC limbs, which extends from the eastern North Atlantic Basin to the Iceland Basin and coincides with the maximum N_2O production rates. Water mixing and basin scale remineralization account for 72% of variation in the observed distribution of N_2O. The mixing-corrected stoichiometric ratio $N_2O:O_2$ for the North Atlantic basin of 0.06 nmol/µmol is in agreement with ratios of $N_2O:O_2$ for local N_2O anomalies, suggesting than up to 28% of N_2O production occurs in the temperate and subpolar Atlantic, an overlooked region for N_2O cycling. Overall, our results highlight the importance of taking into account mixing, O_2 undersaturation when water masses are formed and the increasing atmospheric N_2O concentrations when parameterizing $N_2O:O_2$ and biological N_2O production in the global oceans.

1. Introduction

Nitrous oxide (N_2O) is a gaseous compound that poses a double threat to the Earth's climate. First, it is the third most important anthropogenic greenhouse gas [Prather *et al*., 2012], and second, it has become the most important stratospheric ozone-depleting compound since the drastic reduction of chlorofluorocarbon (CFC) emissions [Ravishankara *et al*., 2009]. Due to human activities, the atmospheric concentration of N_2O is currently 20% higher than pre-industrial levels, increasing from about 271 ppb in 1750 to 324.1 ppb in 2011 [Ciais *et al*., 2013]. The atmospheric concentration of N_2O is determined by the natural balance between land and ocean sources and photolytic destruction of N_2O in the atmosphere [Crutzen, 1970]. According to the latest IPCC Assessment Report [Ciais *et al*., 2013], the global ocean contributes 10–30% to the natural sources of N_2O in the atmosphere.

Hitherto, the main microbial mechanisms identified in N_2O production in the ocean are ammonium oxidation during nitrification and nitrite reduction during denitrification and nitrifier-denitrification, while the main oceanic N_2O consumption process is reduction during denitrification [Cohen, 1978; Cohen and Gordon, 1978; Goreau *et al*., 1980]. These microbial processes are constrained by biological activity and the ambient oxygen (O_2) concentration [Goreau *et al*., 1980]. Under oxic conditions (O_2 above 20 μM), as in most of oceans, N_2O formation occurs via nitrification, whereas under suboxic to anoxic conditions, denitrification is the dominant process. As suboxic and anoxic conditions in the ocean account for only a small percentage of the total ocean volume [Bianchi *et al*., 2012], nitrification has been identified as the main mechanism, contributing up to 93% of global oceanic N_2O production [Freing *et al*., 2012].

Production of N_2O and consumption of O_2 are closely tied, with a strong correlation between the concentration of N_2O and apparent oxygen utilization (AOU). This has led to the development of a range of parameterizations based on field measurements for estimating N_2O production in global biogeochemical models, most of which are based on concentrations, i.e. directly as a function of AOU [Butler *et al*., 1989*;* Nevison *et al*., 2003], while others are based on the oxygen utilization rate (OUR) [Freing *et al.*, 2009] or include variables such as temperature [Butler *et al*., 1989] and depth [Freing *et al*., 2009].

To date, modeling and field observations approaches for computing the global ocean N_2O source and distribution are widely uncertain due to insufficient observations and to incomplete systematic testing of N_2O production and consumption rates, their dependence on O_2 concentrations [Zamora and Oschlies, 2014] and the potential impact of ocean circulation and mixing on oceanic N_2O distribution [Nevison *et al*., 2003*;* Martinez-Rey *et al*., 2015]. Furthermore, studies on the oceanic N_2O cycle have been focused on only a few regions, such as tropical and subtropical gyres of the Pacific Ocean, the Arabian Sea, the Black Sea, the Bedford Basin and the Scheldt estuary, from which information has been used to derive and test model parameterizations [Elkins *et al*., 1978*;* Yoshida *et al*., 1989*;* Fauzi *et al*., 1993*;* Bange *et al*., 2000*;* de Wilde and de Bie, 2000*;* Punshon and Moore, 2004*;* Westley *et al*., 2006*;* Farías *et al.*, 2007*;* Yamagishi *et al*., 2007*;* Frame and Casciotti, 2010]. Many of these low-oxygenated regions are hot spots of oceanic N_2O production and consumption but may not be representative of other ocean environments. However, information on the vertical distribution of N_2O in the Atlantic Ocean is sparse, with first studies from the 70s [Junge and Hahn, 1971], and later studies published by Oudot *et al*. [2002], Walter *et al.* [2006], Forster *et al.* [2009], Ryabenko *et al.* [2012] and Frame *et al.* [2014] among others. The biased geographic distribution of N_2O observations and the lack of attention to ventilated oceanic

regions such as the North Atlantic may have skewed O_2-derived parameterization, which has failed for reproducing N_2O distribution in some ventilated regions [Freing *et al.*, 2012].

The OVIDE section in the North Atlantic has been occupied once every two years since 2002 as part of the World Ocean Circulation Experiment and CO_2/Climate Variability and Predictability Research Repeat Hydrographic programs. In 2012, N_2O measurements were added to the set of properties studied in the OVIDE section. The high-quality physical and biogeochemical decadal database available for this section, in combination with novel N_2O measurements provide a unique opportunity for estimating open-ocean N_2O production rates in the North Atlantic Ocean. The objective of this study was to determine the influence of water mass ventilation, advection and mixing in the eastern North Atlantic on variation in N_2O and on the mechanisms that drive N_2O distribution and production in the region. A constrained least-squares analysis of North Atlantic water masses was performed to separate the role of physical and biogeochemical processes on the distribution of N_2O and O_2, as the basis for reassessing the N_2O:O_2 stoichiometric ratio.

2. Data and methods

2.1 Hydrographic setting of the OVIDE section

The OVIDE section was conceived as an experiment for evaluation of the changes in the Atlantic meridional overturning circulation (AMOC) and in ocean ventilation. The upper limb of the AMOC is driven by the North Atlantic current, which carries warm and saline waters from the subtropics towards the north-east Atlantic (Figure 1). The main contributors to the upper limb of the AMOC are the warm Eastern North Atlantic Central Waters (ENACW) [Iselin, 1936], which occupy the upper part of the OVIDE section from the Iberian Peninsula to the Reykjanes Ridge, with a minor contribution of salty Mediterranean water (MW). The North Atlantic current is gradually cooled during its northward transit and

bifurcates into two main branches eastward of the Charlie-Gibbs fracture zone, one flowing towards the Nordic Seas and the other towards the Iceland Basin, where Subpolar Mode Water (SPMW) is formed [McCartney and Talley, 1982*;* Tsuchiya *et al*., 1992]. The hydrographic properties of SPMW change along the path of the North Atlantic current from subtropical to subpolar regions due to air–sea interactions [McCartney and Talley, 1982; Brambilla and Talley, 2008], leading to a continuous transition of SPMW varieties. Once SPMW reaches the Labrador Sea, it is involved in deep convection processes that lead to the formation of Labrador Sea Water (LSW), which is traceable by its relatively low salinity and high O_2 content [Talley and McCartney, 1982*;* Tsuchiya *et al.*, 1992]. Another water mass detectable in the OVIDE section is the Subarctic Intermediate Water (SAIW), which originates in the western boundary of the subpolar gyre by mixing of the warm saline waters of the North Atlantic current with cold, fresher LSW [Arhan, 1990]. Its signal in the OVIDE section spreads southwards in the upper 500 m, south of Reykjanes Ridge [Pollard *et al*., 2004; García-Ibáñez *et al*., 2015]. Finally, the deep, cold Norwegian Sea waters overflow across the Denmark and Iceland Straits and entrain the warmer SPMW and LSW, forming Denmark Strait Overflow Water (DSOW) and Iceland–Scotland Overflow Water (ISOW), which, with LSW, constitute the North Atlantic Deep Water, the main contributor to the lower limb of the AMOC [Dickson and Brown, 1994]. All the water masses described above include admixtures of waters that we used in the optimum multiparameter (OMP) analysis for proper characterization of the source water types (SWT) that occupy the OVIDE section (see supplementary information).

2.2 The OVIDE 2012 cruise and biogeochemical measurements

The data presented here were collected between Portugal and Greenland on the OVIDE section between 23 June and 20 July 2012 (Figure 1) on board the R/V *Sarmiento de Gamboa*. At each station, temperature and salinity profiles were obtained with a SeaBird 911 Plus CTD Probe, followed by seawater sampling with Niskin bottles for at least 24 levels. Discrete seawater samples were taken (in the following order) for dissolved CFC-11 and CFC-12, O_2, N_2O, and nutrients (NO_3, PO_4 and SiO_2).

FIGURE 1

Triplicate samples for measuring N_2O were collected in 120-mL serum vials, sealed with grey-butyl rubber septa and aluminum crimps and then preserved with saturated $HgCl_2$ to inhibit microbial activity until analysis in the gas chromatography laboratory of the Marine Research Institute (IIM-CSIC) in Vigo (Spain), as described by de la Paz *et al.* [2015]. Briefly, dissolved N_2O was analyzed by static-head space equilibration and determined by gas chromatography (Agilent 7890-GC), separated on a Porapak Q packed column operated at 60 ºC and detected by electron capture detection. The precision of the method, estimated from the coefficient of variation based on replicate analyses, was 0.4%. Dissolved N_2O concentrations were determined by applying the expressions for solubility of Weiss and Price [1980] and expressed in nmol kg^{-1}.

Seawater samples for CFC analysis were drawn into 100-mL glass ampoules, which were flame-sealed on board under an atmosphere of ultraclean nitrogen to avoid air contamination of the samples. CFC-11 and CFC-12 concentrations were determined by gas chromatography in the tracer laboratory at the University of Bremen by the procedure described by Bulsiewicz *et al.* [1998]. The accuracy for both CFC-11 and CFC-12 was 1.4% or 0.005 pmol kg^{-1}, whichever was greater.

Seawater samples were analyzed on board for nutrients with a Skalar Auto-Analyzer, following the classic protocols and methods described by Grasshoff *et al*. [1983] and Álvarez-Salgado *et al.* [1992]. The precision for NO_3, PO_4 and SiO_2 was evaluated as 0.2, 0.02 and 0.1 μmol kg^{-1}, respectively.

O_2 samples were taken in sealed glass flasks and stored in darkness for 24 h before analysis by Winkler potentiometric titration, as described by Culberson [1991], with a precision better than 1 μmol kg^{-1}.

As the OVIDE section crosses a region of intense overturning, neutral density (γ_n) rather than potential density was used to track the direction of motion of water parcels and the direction of along-isopycnal mixing [Talley *et al*., 2011]. The γ_n eliminates the apparent density inversion in the subpolar gyre and also removes the requirement for multiple reference levels. γ_n values were computed according to the algorithms of Jackett and McDougall [1997] (http://www.teos-10.org/preteos10_software/neutral_density.html) on the basis of temperature, salinity, pressure, and geographical location.

2.3 Extended optimum multiparameter (eOMP) water mass analysis

The magnitudes of changes in ocean properties are determined by physical mixing and biogeochemical processes [Anderson and Sarmiento, 1994]. In this study, these changes were analyzed with an OMP analysis, which considers that the observed (physical and/or chemical) properties of a given water sample can be formulated as a linear combination of a finite number of SWTs. The SWTs are characterized by a combination of temperature, salinity, nutrients, O_2 and other tracer values. Therefore, the main goal of an OMP analysis is to calculate the SWT proportions that contribute to each water sample. After the proportions of each SWT *i* for each water sample *j* ($X_{i,j}$) have been computed, the extended version of OMP analysis (eOMP) [Karstensen and Tomczak, 1998] makes it possible to assess

biological influences on non-conservative properties and to compute the O_2 anomaly due to remineralization of organic matter ($\Delta O_{2_{bio}}$), which is calculated using the Redfield-like stoichiometric ratios (see supplementary information). The water masses present in the OVIDE section have been already evaluated in previous studies by means of an eOMP analysis [Álvarez *et al*., 2004, García-Ibáñez *et al.*, 2015]. In this study, we used the results of the eOMP analysis performed by García-Ibáñez *et al.* [2015] (for more details see SI.1). The OMP analysis was restricted to water samples with pressure > 100 dbar to avoid the non-conservative behavior of potential temperature (θ), and salinity in the surface layer due to air-sea interactions after the last maximum of winter convection. The eOMP analysis is reliable since it explains 99% of the changes in the conservative tracers, and, the standard deviation of the residuals (SDR) remains slightly higher than the corresponding analytical errors of the measurements (Table S1) [García-Ibáñez *et al*., 2015]. Previous studies using eOMP analysis provided valuable information in the OVIDE section, such as the relative contribution of the water masses to the interannual variation in the AMOC [García-Ibáñez *et al*., 2015] and the quantitative role of the AMOC in the dissolved organic carbon pool [Fontela *et al.*, 2016].

2.4 Water mass averaged concentrations of N_2O and O_2 in the OVIDE section

The averaged concentration of any chemical parameter (A) for each of the 11 SWTs identified in this study was computed using a multiple linear regression as described by Pérez *et al*. [1993] and Reinthaler *et al.* [2013]. We performed an inversion of a system of 475 equations (the number of N_2O samples below 100 dbar) and 11 unknowns (A_i^{MT}):

$$A_j = \sum_i^{11} X_{i,j}\, A_i^{MT} + \xi_j \qquad j = 1 \text{ to } 475 \text{ samples} \quad (1),$$

where A_j is the measured concentration of A in water sample j, A_i^{MT}, is the "mixing type" property that is equal to the averaged concentration of A in the SWT i, $X_{i,j}$ is the water mass

fraction obtained through the eOMP and ξ_j is the residual. The equation 1 was applied to the entire set of measured concentrations of N_2O and O_2. It is noteworthy that A_i^{MT} values for conservative parameters (θ and salinity) reproduce the conditions in the area where they were defined, it is, they are identic to the A_i^{SWT} terms in the eOMP analysis. However, the A_i^{MT} values for non-conservative parameters reproduce both: (i) the properties in the formation areas of the SWTs (i.e. the initial preformed concentrations, A^0), and (ii) the property changes because of basin-scale remineralization processes accounted from the formation area to the OVIDE section [Pérez *et al*., 1993*;* Álvarez-Salgado *et al*., 2013]. In fact, when equation (1) is applied to AOU (a non-conservative variable), the summation term on the right hand side (the mixing term) represents the change in AOU due to mixing of the water masses within the formation areas, and the residual (second term of the right hand side) describes the AOU change due to the local remineralization process in the section.

Local biogeochemical variability, i.e. biogeochemical differences between samples with the same SWT composition, is expressed in the residuals of equation (1), ξ, which represent the portion of *A* that cannot be modeled by mixing of SWTs and/or basin-scale remineralization. Hereafter, the residuals are referred to as ξA (further details in supplementary information). The higher the correlation coefficient (r^2) of the measured A_j concentration versus that obtained as the sum of the contributions by mixing of the individual types ($\sum_i^{11} X_{i,j}\, A_i^{MT}$) and the lower the SDR (see Table 1), the larger the impact of SWT mixing on the distribution of parameter *A*. Furthermore, to assess the robustness of the ξA term as a proxy of local remineralization, we evaluated the impact derived from uncertainty of the water mass fraction ($X_{i,j}$) in the ξA term. To do this, we performed a perturbation test of equation (1) in which the values of $X_{i,j}$ were modified introducing normally distributed random numbers within a 10% uncertainty of $X_{i,j}$, which doubles the mean error of $X_{i,j}$ and comprise the 90% of the accounted water masses in the eOMP analysis (see Table S.1, and SI.2). The SDR due to

water mass fraction in computing the local biologically produced N_2O (i.e. ξN_2O) is 0.037 nmol kg^{-1} and 0.65 μmol kg^{-1} for the O_2 consumption (ξO_2).

Previous studies used similar numerical approach to assess local and basin-scale remineralization, and the Redfield ratios in the North Atlantic Ocean and in the Southern Ocean [Pérez *et al*., 1993; Brea *et al*., 2004*;* Álvarez-Salgado *et al*., 2013] and to investigate microbial activity in North-East Atlantic Deep Water [Reinthaler *et al*., 2013].

2.5 Transient time distribution method

Increases in atmospheric N_2O must be considered in order to distinguish the fraction of N_2O derived from biotic processes from that of non-biotic origin related to equilibrium with atmospheric N_2O when water masses are formed. The transient time distribution (TTD) method computes the mean age of water masses and the equilibrium N_2O concentration (N_2O_{eq}) with a time-dependent atmospheric N_2O mixing ratio (X_{N_2O}). The method is based on the assumption that any water parcel in the ocean interior consists of many infinitesimal fluid elements of different ages or transit times (time elapsed since the fluid element left the surface mixed layer). The general form of the TTD method is expressed as:

$$C(x,t) = \int_0^\infty C_0(t - t')G(x,t')\,dt' \quad (2),$$

where $C(x,t)$ is the concentration of any dissolved constituent in the ocean interior, C_0 is the time-dependent concentration of the constituent in the surface mixed layer, $(t\text{-}t')$ is the time elapsed since the water parcel was last in contact with the atmosphere (i.e. the age of the water sample), and $G(x,t')$ is the Green function, which propagates the surface concentration into the interior ocean. $G(x,t')$ is approximated by a TTD function given by an 1d-inverse Gaussian age distribution [Waugh *et al.*, 2004], where two parameters have to be determined: the mean age (Γ) and the width of the distribution (Δ):

$$G(t) = \sqrt{\frac{\Gamma^3}{4\pi\Delta^2 t^3}}\, e^{\left(\frac{-\Gamma(t-\Gamma)^2}{4\Delta^2 t}\right)} \quad (3).$$

In simultaneous CFC-11 and CFC-12 measurements, unique determination of both Γ and Δ is not possible [Waugh *et al., 2004*]. If a constant ratio of the two parameters Δ and Γ is assumed, the TTDs can be determined from one tracer alone (e.g. CFC-11 or CFC-12). Using other tracers (tritium and helium-3), Waugh et al. [2004] found that the ratio of Δ/Γ is about unity in the subpolar North Atlantic. On this assumption, Γ=Δ can be inferred from equation (2) with CFC-11 and/or CFC-12 data. Here, we used CFC-12 data (when available, otherwise CFC-11) for the age calculation, as the concentration of CFC-11 in the atmosphere decreased after the mid-1990s, resulting in a non-unique relation between mean age and CFC-11 concentration in younger waters. Waugh *et al*. [2006] applied this approximation to estimate the distribution of anthropogenic CO_2 and its inventories. Subsequently, Freing *et al.* [2009] used the TTD technique to compute N_2O captured during water mass formation on a time-varying atmospheric N_2O, in contrast to the common practice of using the current or a constant N_2O atmospheric concentration [Walter *et al*., 2006]. According to Freing *et al.* [2009], N_2O_{eq} can be calculated as the integral of values of X_{N_2O} multiplied by their respective solubility concentrations ($H_{S,T}$):

$$[N_2O]_{eq}^{TTD}(t) = \int_0^\infty H_{S,T}\, X_{N_2O}(t-t')G(t')\, dt' \quad (4).$$

For the history of X_{N_2O}, we used a combination of ice-core and firm data from Machida *et al.* [1995] for the period 1750–1850 and the polynomial equation used by Freing *et al.* [2009] for 1850 onwards. N_2O solubility was computed from the expression of Weiss and Price [1980].

As the production of N_2O in the ocean is mediated by microbial activity, the departure of observed N_2O above atmospheric equilibrium (ΔN_2O), known as apparent N_2O production, is commonly used as a proxy for the biotic N_2O produced since the water mass was last in contact with the atmosphere [Yoshinari, 1976*;* Nevison *et al*., 2003]. In this study, we

calculated ΔN_2O as:

$$\Delta N_2O = [N_2O]_{obs} - [N_2O]_{eq}^{TTD} \quad (5),$$

where $[N_2O]_{obs}$ is the measured N_2O concentration and $[N_2O]_{eq}^{TTD}$ is computed by applying the TTD method (equation 4) to account for the increase in atmospheric N_2O since pre-industrial times.

2.6 Calculation of apparent production rates of N_2O and O_2

The TTD method also enables calculation of the mean age of water masses, thereby allowing to estimate of the N_2O production rate (N_2O_PR), calculated as:

$$N_2O\_PR = \frac{\Delta N_2O}{\Gamma} \quad (6),$$

where Γ is the TTD calculated mean age of the water sample, and N_2O_PR is the average production rate the water parcel has experienced since its last contact with the atmosphere.

Similarly, the apparent OUR was computed by two approaches:

$$OUR_{AOU} = \frac{AOU}{\Gamma} \quad (7) \text{ and } OUR_{OMP} = \frac{\Delta O_{2_{bio}}}{\Gamma} \quad (8).$$

OUR_{AOU} was used to evaluate the OUR from the AOU, whereas OUR_{OMP} was calculated with the $\Delta O_{2_{bio}}$ term from the eOMP analysis. $\Delta O_{2_{bio}}$, unlike the AOU, takes into consideration the O_2 disequilibrium when the water mass is formed (see supplementary information). Samples from the upper 100 dbar and those with negative rates were excluded to avoid interference with biased CFC measurements in recently formed waters and with non-biotic processes that can affect measured N_2O or O_2, such as air–sea exchange and solubility changes due to the seasonal temperature cycle.

3. Results and discussion

3.1 Vertical distribution of thermohaline properties, O_2 and N_2O in the OVIDE section

The main water masses in the section were identified from the thermohaline and

hydrodynamic settings in previous studies in the OVIDE section (Table 1) [Alvarez *et al*., 2004; García-Ibáñez *et al*., 2015] and are shown in the salinity profile (Figure 2a).

The most remarkable feature of the distributions of θ and salinity is the pronounced vertical gradient, which can be linked to the upper and lower limbs of the AMOC (Figure 2a,b). The limit between the two limbs, represented by γ_n = 27.75 [Lherminier *et al*., 2010], becomes progressively shallower northwards, moving from 1100 m depth in the eastern North Atlantic Basin to 100 m depth in the Irminger Sea. The upper limb of the AMOC is constituted by the warm ENACW and the salty MW in the eastern North Atlantic Basin, by SPMW in the Iceland Basin and by SAIW in the Irminger Sea. Overall, the lower limb of the AMOC in the OVIDE section consists largely of LSW, with some minor contributions of ISOW and DSOW at the bottom layer of the northerly stations and of the North-East Atlantic Deep Water that fills the eastern North Atlantic Basin from 2000 m depth to the bottom. The extreme thermohaline values registered in the section include maximum salinity (S = 36.28) in MW and minimum salinity (S = 34.85) in SAIW, while the warmest and coolest water masses are ENACW (θ = 16 ºC) and DSOW (θ = 1.3 ºC), respectively.

FIGURE 2

The O_2 distribution shows a marked northwest–southeast gradient (Figure 2c) that is highly correlated with ventilation and overturning processes along the section. The combined effects of winter deep convection and the cold temperatures of the water masses when they are formed results in high O_2 values and in a homogeneous vertical O_2 pattern in the water column of the Irminger Sea. The maximum O_2 concentrations (~ 300 μmol kg^{-1}) in the section are observed in the cold, ventilated waters of the Irminger Sea, coinciding with the presence of SPMW of the Irminger (IrSPMW) and DSOW. The southward spread of LSW can be traced by a high O_2 tongue (~ 275 μmol kg^{-1}) centered about 2000 m depth (γ_n ≈

28.00) and extending from the Irminger Sea to the eastern North Atlantic Basin. Overall, the upper limb of the AMOC is characterized by lower O_2 concentrations, with upper layer O_2 values of 225–250 μmol kg^{-1} related to the warm ENACW and minimum O_2 values of about 175 μmol kg^{-1} related to MW, extending around 1000 m depth in the eastern North Atlantic Basin and to minor contributions from SPMW (~ 195 μmol kg^{-1}) in the Iceland Basin.

The spatial distribution of N_2O is shown in Figure 2d. In the surface layer of the OVIDE section, lower N_2O values are observed in the eastern North Atlantic Basin in the warm ENACW (~7.5 nmol kg^{-1}), which increase northwards as the water cools, reaching N_2O concentrations near 10.1 nmol kg^{-1} in the surface layer of the Irminger Sea. A striking feature of N_2O distribution is the tongue of high concentrations (14–16 nmol kg^{-1}) between 600 and 1200 m depth in the eastern North Atlantic Basin, which rises above γ_n = 27.75 in the Iceland Basin. Below this maximum, the N_2O concentration remains relatively homogeneous down to the bottom and close to N_2O saturation, with moderate N_2O values below 1300 m depth related to cold waters filling the lower limb of the AMOC and average N_2O concentrations of 12.6 ± 0.3 nmol kg^{-1} at 3.0 ± 0.9 ºC. The N_2O concentrations measured in this study are consistent with previous findings in the North Atlantic by Walter *et al.* [2006] and Forster *et al.* [2009], which range between 7.6 nmol kg^{-1} in surface northern latitudes and 17 nmol kg^{-1} in the 600-1000 m depth layer of the subtropical Atlantic. Walter *et al.* [2006] also detected the presence of MW as a salty warm tongue at 1000 m depth in the eastern North Atlantic, with no apparent influence on N_2O concentrations, and a nearly constant vertical pattern for N_2O below 2000 m depth. Several questions arise, however, from this analysis of N_2O distribution in the OVIDE section. Why does the N_2O not match the O_2 distribution, as usually observed in oxic oceanic environments? What is the origin of the N_2O concentrations observed in the North Atlantic?

3.2 Reassessment of N_2O and O_2 stoichiometric ratios in the North Atlantic: impact of mixing

The N_2O and O_2 concentrations observed in the interior ocean are not a function of local processes but result from the interaction of circulation dynamics and the remineralization that a water parcel experiences after its formation. The AOU is widely used to infer respiration in the ocean in the basis of the assumption that the surface O_2 concentration is close to saturation with the overlying atmosphere. Nevertheless, significant O_2 disequilibrium has been observed in the high-latitude surface oceans where deep waters are formed [Ito *et al*., 2004], a characteristic feature of the North Atlantic subpolar gyre. We evaluated the effects of different approaches to estimating biological O_2 consumption on the N_2O:O_2 stoichiometric ratio. One approach is based on the AOU and the second on $\Delta O_{2_{bio}}$ computed by eOMP analysis (see supplementary information). AOU, $\Delta O_{2_{bio}}$ and ΔN_2O are used to estimate the biological signal since a water mass was formed, but they cannot discern whether the signal was transported or produced along the OVIDE section.

The vertical distribution of ΔN_2O along the OVIDE section (Figure 3a) shows a tongue of high ΔN_2O (> 4 nmol kg^{-1}) around 500–1000 m depth in the eastern North Atlantic Basin, which propagates northwards above γ_n = 27.75 and occupies the domain of ENACW, MW and SPMW. This high ΔN_2O tongue does not reach the Irminger Sea, consistent with the findings of Walter *et al.* [2006], who suggested that the biological production of N_2O is inhibited in the Irminger Sea by high O_2 concentrations and low temperatures. It is noteworthy that, although MW has no apparent influence on N_2O concentrations (Figure 2d), it makes a moderate contribution to ΔN_2O. Outside of this tongue, the ΔN_2O values are in the range 0–2 nmol kg^{-1}, indicating that the observed N_2O concentrations in the surface layer and below 1500 m depth are driven by temperature-solubility.

The vertical distribution of $\Delta O_{2_{bio}}$ (Figure 3b) resembles that of the ΔN_2O, with

homogeneous values of 0–20 µmol kg^{-1} along the section disrupted by a tongue of high $\Delta O_{2_{bio}}$ that propagates northwards from the eastern North Atlantic Basin, with $\Delta O_{2_{bio}}$ values in the core of the tongue of 80–95 µmol kg^{-1}. A comparison of O_2 and $\Delta O_{2_{bio}}$ (Figure 2c and 3b, respectively) shows that high O_2 concentrations in the lower limb of the AMOC are driven by physics and solubility rather than by biology. While AOU shows a similar distribution to $\Delta O_{2_{bio}}$ in the upper 2000 m, it differs markedly below 2000 m depth in the eastern North Atlantic Basin, where NEADW dominates (Figure 2a). In NEADW, the AOU values are around 90 µmol kg^{-1} whereas $\Delta O_{2_{bio}}$ remains below 20 µmol kg^{-1}. The differences are due to the origin of this water mass. NEADW is formed from various entrainments during the passage of ISOW through the Iceland Basin [van Aken, 2000] and recirculation in the eastern North Atlantic Basin, where it mixes with the surrounding waters, including Antarctic Bottom Waters (AABW) with a low O_2 content [van Aken and Becker, 1996]. Differences in AOU-$\Delta O_{2_{bio}}$ are found not only in NEADW, but also in deep waters of the Iceland Basin and the Irminger Sea (averaged differences of 35 µmol kg^{-1} at z > 1800 m), due to O_2 undersaturation of deep water contributors. The largest surface–ocean O_2 disequilibrium occurs in high-latitude subduction regions, where deep water forms. Deep water is formed in both the Southern Ocean (forming AABW) and the northern North Atlantic and Nordic Seas (forming LSW and precursor water masses of ISOW and DSOW). At 50 m depth, the annual mean O_2 saturation is 86% in the Southern Ocean and 96% in the northern North Atlantic [Duteil *et al*., 2013]. $\Delta O_{2_{bio}}$ takes into consideration the preformed properties of water masses and is equivalent to true oxygen utilization, as defined by Ito *et al.* [2004], providing a more realistic tracer of biological O_2 consumption. Recently, Duteil *et al*. [2013] compared six coupled-circulation biogeochemical ocean models and reported AOU-based estimates of O_2 consumption more than 25% higher than the true oxygen utilization.

In the OVIDE section, the main result of the distribution of ΔN_2O, reinforced by the

distribution of $\Delta O_{2_{bio}}$, is the higher impact of biological production on the observed N_2O concentrations in the upper limb than in the lower limb of the AMOC, in which N_2O concentrations reflect the colder temperatures.

FIGURE 3

We also used combined measurements of CFCs and N_2O to assess the effect of different approaches to calculating saturation N_2O concentrations. The current approach ($X_{atm_{N_2O}}$ = 325 ppb in 2012; National Oceanic and Atmospheric Administration) produces higher $[N_2O]_{eq}$ and lower ΔN_2O values than the TTD-CFCs approach. The differences range from 0 to 1 nmol kg^{-1} above 2000 m depth and increase to 2 nmol kg^{-1} below 2000 m depth, resulting in overestimates of up to 18% in $[N_2O]_{eq}$, in agreement with the range of 8–13% given by Freing *et al.* [2009] for the North Atlantic. As the ΔN_2O is higher in the subsurface ocean [Nevison *et al.*, 2003], the approach that we selected has a quantitatively minor impact on estimates of biological production of N_2O; nevertheless, for waters deeper than 2000 m, the current approach leads to inconsistent negative values of ΔN_2O.

Since the early studies on N_2O cycling, the mechanisms of N_2O production have been evaluated as correlations between O_2 consumption, in terms of AOU, and N_2O production [Yoshinari, 1976; Goreau *et al.*, 1980], a positive correlation indicating nitrification and a negative correlation denitrification. The N_2O yield per O_2 molecule respired was assessed from the slope of the correlation. There are other biological pathways that could produce N_2O in aerobic environment such as nitrifier-denitrification that is enhance in low O_2 environments [Frame and Casciotti, 2010], but this mechanism can be considerate very improbable in our study region. We evaluated the uncertainties associated with using AOU for estimating the stoichiometric ratio N_2O:O_2. In the OVIDE section, both $\Delta O_{2_{bio}}$ and AOU show a positive correlation with ΔN_2O, indicating that nitrification is the main mechanism for

production of N_2O in the North Atlantic (Figure 4). However, the slopes and distribution patterns of the pairs $\Delta N_2O/\Delta O_{2_{bio}}$ and ΔN_2O/AOU show marked differences. For the entire water column, the slope of the linear relationship $\Delta N_2O/\Delta O_{2_{bio}}$ is 0.0586 (r^2 = 0.94; n = 474), which is higher and less uncertain than when AOU is used as the reference for O_2 consumption, when the slope of ΔN_2O/AOU is 0.0346 (r^2 = 0.38; n = 474). For the waters of the upper and lower limbs of the AMOC separately, the slopes of both $\Delta N_2O/\Delta O_{2_{bio}}$ and ΔN_2O/AOU are 0.0591 for the upper limb (γ_n < 27.75; $\Delta N_2O = 0.0591*\Delta O_{2_{bio}} - 0.153$, r^2 = 0.95; ΔN_2O = 0.0591*AOU – 0.639, r^2 = 0.93), while for the lower limb the slope for $\Delta N_2O/\Delta O_{2_{bio}}$ is 0.054 (γ_n > 27.75; $\Delta N_2O = 0.0544*\Delta O_{2_{bio}} - 0.226$, r^2 = 0.88) and the linear correlation is not significant for ΔN_2O/AOU. These results indicate that, when the O_2 saturation in preformed properties is considered, the stoichiometric ratio $\Delta N_2O/\Delta O_{2_{bio}}$ applies to the entire water column. This suggests that the double distributions in the plot of the correlation between ΔN_2O and AOU previously reported for the North Atlantic [Walter *et al*., 2006; Freing *et al*., 2009] are probably due to biased use of AOU for ventilated waters and not to nitrification processes. Our estimated ratios for the upper 2000 m are in agreement with those reported previously for the North Atlantic [Nevison *et al*., 2003; Walter *et al.*, 2006; Freing *et al*., 2009]. Nevison *et al.* [2003] acknowledged the impact of mixing in the correlation of ΔN_2O/AOU, and obtained a mixing corrected slope of 0.06 nmol μmol^{-1} after applying a simple end-member mixing model. Despite the agreement in stoichiometric ratios, the degree of uncertainty in the results of Nevison *et al.* [2003] results is considerably higher than with our eOMP approach.

FIGURE 4

The processes that contribute to N_2O concentrations in the ocean are complex, although dissolved O_2 has been identified as the most important factor from empirical observations,

theoretical considerations and laboratory measurements [Nevison *et al*., 2003]. Besides O_2 levels, most of the parameters used in biogeochemical models for the N_2O:O_2 ratio include a term to modulate N_2O production based on temperature and/or depth, in order to obtain a formula to reproduce the lower N_2O concentrations in deep waters [Butler *et al*., 1989; Nevison *et al.*, 2003; Freing *et al*., 2009]. Some authors [Zamora *et al*., 2012] have called for reassessment of the dependence of the ΔN_2O:AOU ratio on temperature and depth, as no clear model or observational evidence has been provided. Furthermore, the biotic ΔN_2O:AOU ratio reflects the integrated history of the depths of the water mass rather than its current depth, so that this ratio is an imperfect measure for testing a depth or temperature dependence hypothesis [Zamora *et al*., 2012]. Our study reinforces the idea that parameterizations as a function of depth or temperature should be reviewed, including use of AOU, which is a biased parameter for evaluating biological activity in ventilated oceanic regions.

3.3 Production of N_2O from basin to local scale; transported versus in-situ biological N_2O production in the North Atlantic

Equation (1) allowed us to objectively separate the effect of water mass mixing and basin-scale remineralization (from the formation area to the center of mass of the 11 water masses) from the effect of local scale processes around the center of mass of each water mass. Comparison of the measured N_2O and O_2 concentrations with those obtained as the sum of the contributions of the individual water masses (i.e. eq. (1): $\sum_i^{11} X_{i,j}\, A_i^{MT}$) indicates that conservative mixing and basin-scale remineralization explain 87% of the total change in dissolved O_2 and 72% of that for N_2O (see Table 1). Therefore, a considerable fraction of the changes in N_2O and O_2 concentrations can be explained by local scale differences in the degree of remineralization, which information is contained in ξN_2O and ξO_2 (up to 13% for O_2 and 28% for N_2O). The robustness of the eOMP analysis and the $X_{i,j}$ used in equation (1) were tested by García-Ibáñez *et al*. [2015] thought a perturbation analysis of the uncertainties

(more detailed in text SI.1). The resulting uncertainties in the $X_{i,j}s$ (expressed as per one) ranged between 0.015 and 0.13 (see table S.1). We evaluated the errors in equation (1) using these $X_{i,j}$ uncertainties thought 50 perturbation experiments of equation (1). The SDR for the residuals obtained in the experiment was 0.037 nmol kg^{-1} for N_2O and 0.65 for O_2 µmol kg^{-1} (see residuals distribution in S.2). Furthermore, the SD of the estimated local-biological signal was 0.7 nmol kg^{-1} for ξN_2O and 28.5 µmol kg^{-1} for ξO_2, which are about one order of magnitude larger than the corresponding analytical errors (0.05 nmol kg^{-1} for N_2O and 1 µmol kg^{-1} for O_2) and than the errors derived from uncertainty in $X_{i,j}$. Therefore, the impact of local non-conservative biogeochemical processes is still considerable.

Analysis of the distribution of residuals from equation (1), ξN_2O and ξO_2, yields further insights into the mechanisms of the changes in N_2O and O_2, which is related to areas of relative intense/weak remineralization or ventilation. Such areas have been identified in figure 5. The positive or negative magnitude of the residuals depend on their relative values compared to the mixing type property (A_i^{MT}). Hence, the sign of the residuals is related with the nature of local processes: positive-ξN_2O/negative-ξO_2 values are due to locally enhanced remineralization, and contrarily, negative-ξN_2O/positive-ξO_2 are due to local ventilation or relatively weak remineralization within the spatial dominion of each water mass. The vertical distribution of ξN_2O and ξO_2 presents a mirrored pattern (opposite sign trends for ξO_2 and ξN_2O), with higher local O_2 consumption/N_2O production above γ_n = 27.75 (52 µmol kg^{-1} O_2: 3.5 nmol kg^{-1} N_2O, Figure 5a,b), coinciding with maximum ΔN_2O and $\Delta O_{2_{bio}}$ (Figure 3a,b). Hence, the net biological N_2O signal captured by ΔN_2O (Figure 3a) is the summation of transported and local remineralization within the section, whereas ξN_2O (Figure 5a) is due only to local biological production of N_2O.

At local scale, the stoichiometric coefficient for O_2 consumption to N_2O production not affected by mixing is obtained from the linear correlation between the residuals ξN_2O and

ξO_2 (Figure 5c). The slope of ξN_2O versus ξO_2 is 0.056 ± 0.001 (r^2 = 0.74), which is the same value obtained for the basin scale after applying the ratio ΔN_2O: $\Delta O_{2_{bio}}$ (Figure 4). Similarly, local biological production was assessed with identical results by using ξAOU or $\xi \Delta O_{2_{bio}}$(see supplementary information). This indicates that local N_2O production, due to mesoscale processes different from SWT mixing, is driven by same mechanisms than at basin scale and that the value of 0.06 for the stoichiometric ratio of N_2O:O_2 is a representative value for the North Atlantic.

FIGURE 5

As the A_i^{MT} properties computed with equation (1) include the effect of biology, O_2^{MT} (Table 1) and N_2O^{MT} address not only the air–sea disequilibrium when water masses are formed but also remineralization processes from the formation area of each water mass to their centers of mass. We also computed the averaged apparent N_2O production and O_2 utilization for each SWT since its formation (ΔN_2O^{MT} and $\Delta O_{2_{bio}}^{MT}$, values in Table 1) by applying equation (1) to the ΔN_2O and $\Delta O_{2_{bio}}$ values of all seawater samples. The relation between ΔN_2O^{MT} and $\Delta O_{2_{bio}}^{MT}$ shows a good linear correlation, with a slope of 0.056 (r^2 = 0.97; nSWT = 11). The stoichiometric ratio for N_2O:O_2 when SWTs are defined reproduces the value obtained for ΔN_2O: $\Delta O_{2_{bio}}$ and the residuals ξN_2O: $\xi \Delta O_2$ (Figures 4 and 5c), thus suggesting that nitrification is responsible for the positive values of ΔN_2O^{MT}. This highlights also the relative degree of homogeneity in the nitrification and its relation with the O_2 in the environment in the North Atlantic Basin. Further analysis of the properties shown in Table 1 indicates that the high N_2O^{MT} content observed in water masses formed by deep convection in the North Atlantic subpolar gyre (i.e. LSW and precursor water masses of ISOW and DSOW) is driven by temperature-solubility (θ < 5 ºC), and, conversely, the lower temperature-solubility in the warmest ENACW drives the lowest N_2O^{MT}. In summary, the most important features of the

North Atlantic are the mixing and southward advection of the atmospheric N_2O imprint in the lower limb of the AMOC, filled by cold, recently ventilated waters. In contrast, the upper limb of the AMOC is dominated by production of N_2O in situ in the Iceland and eastern North Atlantic basins, along with northward transport of mode and central waters enriched with N_2O due to accumulated remineralization in tropical and subtropical latitudes, where higher N_2O contents and O_2 depletion have been reported [Walter *et al*., 2006; Forster *et al*., 2009; Rees *et al*., 2011].

3.4 Estimated N_2O production rates in the OVIDE section

The N_2O_PR varies between 0 and 0.2 nmol kg^{-1} $year^{-1}$ in the OVIDE section, and its distribution (Figure 6a) follows the distribution pattern of ΔN_2O (Figure 3a). The high N_2O_PR values spread along the eastern North Atlantic and Iceland basins between 300 and 1000 m depth correspond to waters younger than 40 years (age determined by the TTD technique) and considerably lower N_2O_PR in the Irminger Sea and generally throughout the water column below 1000 m depth. For $\gamma_n > 27.75$, the average N_2O_PR is 0.016 ± 0.019 nmol kg^{-1} $year^{-1}$, which is nearly one order of magnitude lower than that of the upper limb of the AMOC. Our results fall in the range of estimates by Freing *et al*. [2009] for the Atlantic Ocean and for the upper 500 m of 0.2 nmol kg^{-1} $year^{-1}$ estimated for the global ocean [Freing *et al*., 2012].

FIGURE 6

The OUR estimation based on AOU and on $\Delta O_{2_{bio}}$ derived by eOMP analysis, i.e. OUR_{AOU} and OUR_{OMP}, are shown in the two lower panels of Figure 6. Overall, the distribution pattern of high OURs follows the main trend of N_2O_PR, regardless of the method used; however, important discrepancies are seen between the two approaches. For the whole section, the average value of OUR_{AOU} is 30% higher than that of OUR_{OMP} for $\gamma_n < 27.75$ (OUR_{OMP} = 1.47 ± 0.68 µmol kg^{-1} $year^{-1}$; OUR_{AOU} = 1.92 ± 0.62 µmol kg^{-1} $year^{-1}$) and 200% higher for $\gamma_n >$

27.75 (OUR_{OMP} = 0.38 ± 0.35 µmol kg^{-1} $year^{-1}$; OUR_{AOU} = 1.15 ± 0.65 µmol kg^{-1} $year^{-1}$). The greatest discrepancies between the two approaches are observed for the Irminger Sea, where deep convection causes O_2 undersaturation; consequently, AOU overestimates biological O_2 consumption. The discrepancies are exacerbated when N_2O production integrated over the water column is evaluated, as volumes of water above γ_n = 27.75 are more than three times higher than for γ_n < 27.75. These discrepancies have important consequences, as some authors [Freing *et al.*, 2012] propose that the ratio N_2O_PR:OUR be used instead of ΔN_2O:AOU for estimating global N_2O production. Some authors have pointed out limitations in the OUR despite the method used to compute the O_2 biological utilization due to the non-proportional diffuse mixing of AOU (or $\Delta O_{2_{bio}}$) and water mass age [Mecking *et al.*, 2004; Koeve and Kähler, 2016]. Although there is not at present a perfect method to estimate the biogeochemical rates, OUR has been viewed as the best available method to determine respiration in the ocean interior [Emerson and Hedges, 2008].

We also computed N_2O_PR for the OVIDE section by the parameterization proposed by Freing *et al*. [2009] as a function of OUR_{AOU}, temperature and depth. The average N_2O rate resulting from this approach was about 300% higher for γ_n > 27.75 than our results for N_2O_PR based on N_2O observations and water mass age. The unexpectedly high values of OUR and N_2O_PR in cold, ventilated oceanic regions have been associated with limitations for age estimation by the CFC tracer methods in young water [Freing *et al.*, 2012]. Our study indicates, however, that anomalously high N_2O production rates in the North Atlantic subpolar gyre and in the deep waters of the North Atlantic Ocean result from use of AOU instead of preformed O_2 for estimating biological consumption.

4. Concluding comments

The N_2O database for the North Atlantic and the OMP-derived water mass analysis presented here show a higher impact of biological production on the N_2O concentrations in the upper limb of the AMOC than in the lower limb, where the N_2O concentrations reflect the colder temperatures.

The conservative mixing and basin-scale remineralization explain 87% of the total variation of dissolved O_2 and 72% of that for N_2O. Therefore, a considerable fraction of the variation in N_2O and O_2 concentrations is due to local biological activity in the OVIDE section (up to 13% for O_2 and 28% for N_2O). Analysis of the ratios of the residuals from the conservative mixing, i.e. ξN_2O in relation to ξO_2, reveals, first, that the anomalies are due mainly to remineralization processes, as the calculated ratios are equivalent to the basin-scale ratio $\Delta N_2O{:}\Delta O_{2_{bio}}$, and, secondly, that the positive correlation of $\Delta N_2O{:}\Delta O_{2_{bio}}$ suggests that nitrification is the most likely biological process in N_2O production in North Atlantic water masses and that a value of 0.06 for the stoichiometric ratio of $N_2O{:}O_2$ is homogeneous for the North Atlantic.

The most important features of the North Atlantic are mixing and southward advection of the atmospheric N_2O imprint in the lower limb of the AMOC, filled by cold, recently ventilated waters. In contrast, the upper limb of the AMOC is dominated by the production of N_2O in situ in the Iceland and eastern North Atlantic basins, along with northward transport of mode and central waters enriched with N_2O due to accumulated remineralization in tropical and subtropical latitudes, where higher N_2O content and O_2 depletion have been reported [Walter *et al*., 2006; Forster *et al*., 2009; Rees *et al*., 2011.

Analysis of mixing-corrected stoichiometric ratios of $N_2O{:}O_2$ indicates that parameterization of the ΔN_2O:AOU ratio as a function of temperature and depth should be revised by including the mixing effects and re-evaluating use of AOU for such parameterizations, as it is a biased parameter for evaluating biological activity in ventilated oceanic regions. This study

also shows that both the O_2 disequilibrium of water masses when they are formed and the effect of transient increases in atmospheric N_2O on oceanic N_2O concentrations are key parameters for correctly estimating N_2O oceanic production in global biogeochemical models.

Acknowledgments and data

The authors wish to thank the Captain and the crew of R/V *Sarmiento de Gamboa* for their help during the cruise. We are very grateful to all the scientific team of the CATARINA cruise, and to Fernando Alonso and Anton Velo in particular for their participation in analyzing nutrients and oxygen. Financial support for this work came from the Consejo Superior de Investigaciones Científicas (CSIC) and the Spanish Ministry of Economy and Competitiveness through the CATARINA project (CTM2010-17141) and BOCATS (CTM2013-41048-P) projects both cofounded by the Fondo Europeo de Desarrollo Regional (FEDER), and also from the Ingos EU Project (Grant Agreement 284274) and from Xunta de Galicia through the OSIMON project (09MDS035402PR). The data supporting the conclusions can be obtained in the supplementary information.

References

van Aken, H. M. (2000), The hydrography of the mid-latitude Northeast Atlantic Ocean: II: The intermediate water masses, *Deep Sea Res. Part Oceanogr. Res. Pap.*, *47*(5), 789–824, doi:10.1016/S0967-0637(99)00112-0.

van Aken, H. M., and G. Becker (1996), Hydrography and through-flow in the north-eastern North Atlantic Ocean: the NANSEN project, *Prog. Oceanogr.*, *38*(4), 297–346, doi:10.1016/S0079-6611(97)00005-0.

Álvarez, M., F. F. Pérez, H. Bryden, and A. F. Ríos (2004), Physical and biogeochemical transports structure in the North Atlantic subpolar gyre, *J. Geophys. Res.*, *109*(C03027), doi:10.1029/2003JC002015.

Álvarez-Salgado, X., F. Fraga, and F. Pérez (1992), Determination of nutrient salts by automatic methods both in seawater and brackish water: the phosphate blank, *Mar. Chem.*, *39*, 311–319, doi:10.1016/0304-4203(92)90016-4.

Álvarez-Salgado, X. A., M. Nieto-Cid, M. Álvarez, F. F. Pérez, P. Morin, and H. Mercier (2013), New insights on the mineralization of dissolved organic matter in central,

intermediate, and deep water masses of the northeast North Atlantic, *Limnol Ocean.*, *58*(2), 681–696, doi:10.4319/lo.2013.58.2.0681.

Anderson, L. A., and J. L. Sarmiento (1994), Redfield ratios of remineralization determined by nutrient data analysis, *Glob. Biogeochem Cycles*, *8*(1), 65–80, doi:10.1029/93GB03318.

Arhan, M. (1990), The North Atlantic current and subarctic intermediate water, *J. Mar. Res.*, *48*(1), 109–144, doi:10.1357/002224090784984605.

Bange, H. W., T. Rixen, A. M. Johansen, R. L. Siefert, R. Ramesh, V. Ittekkot, M. R. Hoffmann, and M. O. Andreae (2000), A revised nitrogen budget for the Arabian Sea, *Global Biogeochem. Cy.*, *14*, 1283–1297, doi:10.1029/1999gb001228.

Bianchi, D., J. P. Dunne, J. L. Sarmiento, and E. D. Galbraith (2012), Data-based estimates of suboxia, denitrification, and N_2O production in the ocean and their sensitivities to dissolved O_2, *Glob. Biogeochem. Cycles*, *26*(2), doi:10.1029/2011GB004209.

Brambilla, E., and L. D. Talley (2008), Subpolar mode water in the northeastern Atlantic: 1. Averaged properties and mean circulation, *J Geophys Res*, *113*, C04025, doi:10.1029/2006JC004062.

Brea, S., X. A. Álvarez-Salgado, M. Álvarez, F. F. Pérez, L. Mémery, H. Mercier, and M. J. Messias (2004), Nutrient mineralization rates and ratios in the eastern South Atlantic, *J. Geophys. Res.*, *109*, C05030, doi:10.1029/2003JC002051.

Bulsiewicz, K., H. Rose, O. Klatt, A. Putzka, and W. Roether (1998), A capillary-column chromatographic system for efficient chlorofluorocarbon measurement in ocean waters, *J. Geophys. Res. Oceans 1978–2012*, *103*(C8), 15959–15970, doi: 10.1029/98JC00140.

Butler, J. H., J. W. Elkins, T. M. Thompson, and K. B. Egan (1989), Tropospheric and dissolved N_2O of the west Pacific and east Indian Oceans during the El Niño Southern Oscillation event of 1987, *J. Geophys. Res. Atmospheres 1984–2012*, *94*(D12), 14865–14877, doi:10.1029/JD094iD12p14865.

Ciais, P. et al. (2013), Carbon and other biogeochemical cycles, in *Climate Change 2013: The Physical Science Basis. Contribution of Working Group I to the Fifth Assessment Report of the Intergovernmental Panel on Climate Change. [Stocker, T.F., D. Qin, G.-K. Plattner, M. Tignor, S.K. Allen, J. Boschung, A. Nauels, Y. Xia, V. Bex and P.M. Midgley (eds.)]*. *Cambridge University Press, Cambridge, and New York City, New York,* pp. 465–570.

Crutzen, P. J. (1970), The influence of nitrogen oxides on the atmospheric ozone content, *Q. J. R. Meteorol. Soc.*, *96*(408), 320–325, doi:10.1002/qj.49709640815.

Culberson, C. H. (1991), *WOCE operations manual (WHP operations and methods), WHPO 91/1*, Woods Hole Oceanographic Institute, Woods Hole, Massachusetts.

Dickson, R. R., and J. Brown (1994), The production of North Atlantic deep water: sources, rates, and pathways, *J. Geophys. Res.*, *99*(C6), 12319–12341, doi:10.1029/94JC00530.

Duteil, O., W. Koeve, A. Oschlies, D. Bianchi, E. Galbraith, I. Kriest, and R. Matear (2013), A novel estimate of ocean oxygen utilisation points to a reduced rate of respiration in the ocean interior, *Biogeosciences*, *10*(11), 7723–7738, doi:10.5194/bg-10-7723-2013.

Elkins, J. W., S. C. Wofsy, M. B. McElroy, C. E. Kolb, and W. A. Kaplan (1978), Aquatic sources and sinks for nitrous oxide, *Nature*, *275*(5681), 602–606, doi:10.1038/275602a0.

Emerson, S. R., and J. I. Hedges (2008), *Chemical Oceanography and the Marine Carbon Cycle*, 453 pp., Cambridge Univ. Press, Cambridge, U. K.

Farías, L., A. Paulmier, and M. Gallegos (2007), Nitrous oxide and N-nutrient cycling in the oxygen minimum zone off northern Chile, *Deep Sea Res. Part Oceanogr. Res. Pap.*, *54*(2), 164–180, doi:10.1016/j.dsr.2006.11.003.

Fauzi, R., C. Mantoura, C. S. Law, N. J. P. Owens, P. H. Burkill, E. M. S. Woodward, R. J. M. Howland, and C. A. Llewellyn (1993), Nitrogen biogeochemical cycling in the northwestern Indian Ocean, *Deep Sea Res. Part II Top. Stud. Oceanogr.*, *40*(3), 651–671, doi:10.1016/0967-0645(93)90050-W.

Fontela, M., M. I. García-Ibáñez, D. A. Hansell, H. Mercier, and F. F. Pérez (2016), Dissolved organic carbon in the North Atlantic meridional overturning circulation, *Sci. Rep.*, *6*, 26931, doi:10.1038/srep26931.

Forster, G., R. C. Upstill-Goddard, N. Gist, C. Robinson, G. Uher, and E. M. S. Woodward (2009), Nitrous oxide and methane in the Atlantic Ocean between 50°N and 52°S: Latitudinal distribution and sea-to-air flux, *Deep Sea Res. Part II Top. Stud. Oceanogr.*, *56*(15), 964–976, doi:10.1016/j.dsr2.2008.12.002.

Frame, C. H., and K. L. Casciotti (2010), Biogeochemical controls and isotopic signatures of nitrous oxide production by a marine ammonia-oxidizing bacterium, *Biogeosciences*, *7*(9), 2695–2709, doi:10.5194/bg-7-2695-2010.

Frame, C. H., E. Deal, C. D. Nevison, and K. L. Casciotti (2014), N_2O production in the eastern South Atlantic: Analysis of N_2O stable isotopic and concentration data, *Glob. Biogeochem. Cycles*, *28*, 1262–1278, doi:10.1002/2013GB004790.

Freing, A., D. W. R. Wallace, T. Tanhua, S. Walter, and H. W. Bange (2009), North Atlantic production of nitrous oxide in the context of changing atmospheric levels, *Glob. Biogeochem. Cycles*, *23*(4), GB4015, doi:10.1029/2009GB003472.

Freing, A., D. W. R. Wallace, and H. W. Bange (2012), Global oceanic production of nitrous oxide, *Phil. Trans. R. Soc. B Biol. Sci.*, *367*(1593), 1245–1255, doi:10.1098/rstb.2011.0360.

García-Ibáñez, M. I., P. C. Pardo, L. I. Carracedo, H. Mercier, P. Lherminier, A. F. Ríos, and F. F. Pérez (2015), Structure, transports and transformations of the water masses in the Atlantic subpolar gyre, *Prog. Oceanogr.*, *135*, 18–36, doi:10.1016/j.pocean.2015.03.009.

Goreau, T. J., W. A. Kaplan, S. C. Wofsy, M. B. McElroy, F. W. Valois, and S. W. Watson (1980), Production of NO_2^- and N_2O by nitrifying bacteria at reduced concentrations of oxygen, *Appl. Environ. Microbiol.*, *40*(3), 526–532.

Iselin, C. O. (1936), *A study of the circulation of the western North Atlantic*, Pap. Phys. Oceanogr. Meteorol. Massachusetts Institute of Technology and Woods Hole Oceanographic Institute.

Ito, T., M. J. Follows, and E. A. Boyle (2004), Is AOU a good measure of respiration in the oceans?, *Geophys. Res. Lett.*, *31*, L17305, doi:10.1029/2004GL020900.

Jackett, D. R., and T. J. McDougall (1997), A neutral density variable for the world's oceans, *J. Phys. Oceanogr.*, *27*(2), 237–263, doi:10.1175/1520-0485(1997)027<0237:ANDVFT>2.0.CO;2.

Junge, C., and J. Hahn (1971), N_2O measurements in the North Atlantic, *J. Geophys. Res.*, *76*(33), 8143–8146, doi: 10.1029/JC076i033p08143.

Karstensen, J., and M. Tomczak (1998), Age determination of mixed water masses using CFC and oxygen data, *J Geophys Res*, *103*(C9), 18599–18609, doi:10.1029/98JC00889.

Koeve, W., and P. Kähler (2016), Oxygen utilization rate (OUR) underestimates ocean respiration: A model study, *Global Biogeochem. Cycles*, *30*, 1166–1182, doi:10.1002/2015GB005354

Lherminier, P., H. Mercier, T. Huck, C. Gourcuff, F. F. Perez, P. Morin, A. Sarafanov, and A. Falina (2010), The Atlantic meridional overturning circulation and the subpolar gyre observed at the A25-OVIDE section in June 2002 and 2004, *Deep Sea Res. Part Oceanogr. Res. Pap.*, *57*(11), 1374–1391, doi:10.1016/j.dsr.2010.07.009.

Martinez-Rey, J., L. Bopp, M. Gehlen, A. Tagliabue, and N. Gruber (2015), Projections of oceanic N_2O emissions in the 21st century using the IPSL Earth system model, *Biogeosciences*, *12*(13), 4133–4148, doi:10.5194/bg-12-4133-2015.

McCartney, M. S., and L. D. Talley (1982), The subpolar mode water of the North Atlantic Ocean, *J. Phys. Oceanogr.*, *12*(11), 1169–1188, doi:10.1175/1520-0485(1982)012<1169:TSMWOT>2.0.CO;2.

Mecking, S., C. E. Greene, S. L. Hautala, and R. E. Sonnerup (2004), Influence of mixing on CFC uptake and CFC ages in the North Pacific thermocline, *J. Geophys. Res.*, *109*, C07014, doi:10.1029/2003JC001988.

Nevison, C., J. H. Butler, and J. W. Elkins (2003), Global distribution of N_2O and the ΔN_2O-AOU yield in the subsurface ocean, *Glob. Biogeochem. Cycles*, *17*(4), doi:10.1029/2003GB002068.

Oudot, C., P. Jean-Baptiste, E. Fourre, C. Mormiche, M. Guevel, J. -F. Ternon, and P. Le Corre (2002), Transatlantic equatorial distribution of nitrous oxide and methane, *Deep Sea Res. Part Oceanogr. Res. Pap.*, *49*, 1175–1193, doi: 10.1016/S0967-0637(02)00019-5.

de la Paz, M., I. E. Huertas, S. Flecha, A. F. Ríos, and F. F. Pérez (2015), Nitrous oxide and methane in Atlantic and Mediterranean waters in the Strait of Gibraltar: Air-sea fluxes and inter-basin exchange, *Prog. Oceanogr.*, *138*, *Part A*, 18–31, doi:10.1016/j.pocean.2015.09.009.

Pérez, F. F., C. Mouriño, F. Fraga, and A. F. Rios (1993), Displacement of water masses and remineralization rates off the Iberian Peninsula by nutrient anomalies, *J. Mar. Res.*, *51*, 869–892, doi:10.1357/0022240933223891.

Pollard, R. T., J. F. Read, N. P. Holliday, and H. Leach (2004), Water masses and circulation pathways through the Iceland Basin during Vivaldi 1996, *J. Geophys. Res.*, *109*, C04004, doi:10.1029/2003JC002067.

Prather, M. J., C. D. Holmes, and J. Hsu (2012), Reactive greenhouse gas scenarios: Systematic exploration of uncertainties and the role of atmospheric chemistry, *Geophys. Res. Lett.*, *39*(9), L09803, doi:10.1029/2012GL051440.

Punshon, S., and R. M. Moore (2004), Nitrous oxide production and consumption in a eutrophic coastal embayment, *Mar. Chem.*, *91*(1–4), 37–51, doi:10.1016/j.marchem.2004.04.003.

Ravishankara, A. R., J. S. Daniel, and R. W. Portmann (2009), Nitrous oxide (N_2O): the dominant ozone-depleting substance emitted in the 21st century, *Science*, *326*(5949), 123–125, doi:10.1126/science.1176985.

Reinthaler, T., X. A. Álvarez Salgado, M. Álvarez, H. M. van Aken, and G. J. Herndl (2013), Impact of water mass mixing on the biogeochemistry and microbiology of the Northeast Atlantic Deep Water, *Glob. Biogeochem. Cycles*, *27*(4), 1151–1162, doi:10.1002/2013GB004634.

Ryabenko, E., A. Kock, H. W. Bange, M. A. Altabet, and D. W. R. Wallace (2012), Contrasting biogeochemistry of nitrogen in the Atlantic and Pacific Oxygen Minimum Zones, *Biogeosciences*, *9*(1), 203–215, doi:10.5194/bg-9-203-2012.

Talley, L. D., G. L. Pickard, W. J. Emery, and J. H. Swift (2011), *Descriptive physical oceanography: an introduction.*, 6th Edition., Elsevier, London.

Tsuchiya, M., L. D. Talley, and M. S. McCartney (1992), An eastern Atlantic section from Iceland southward across the equator, *Deep Sea Res. Part Oceanogr. Res. Pap.*, *39*(11), 1885–1917, doi:10.1016/0198-0149(92)90004-D.

Walter, S., H. W. Bange, U. Breitenbach, and D. W. R. Wallace (2006), Nitrous oxide in the North Atlantic Ocean, *Biogeosciences*, *3*(4), 607–619, doi:10.5194/bg-3-607-2006.

Waugh, D. W., T. W. N. Haine, and T. M. Hall (2004), Transport times and anthropogenic carbon in the subpolar North Atlantic Ocean, *Deep Sea Res. Part Oceanogr. Res. Pap.*, *51*(11), 1475–1491, doi:10.1016/j.dsr.2004.06.011.

Waugh, D. W., T. M. Hall, B. I. McNeil, R. Key, and R. J. Matear (2006), Anthropogenic CO_2 in the oceans estimated using transit time distributions, *Tellus B*, *58*(5), 376–389, doi:10.1111/j.1600-0889.2006.00222.x.

Weiss, R. F., and B. A. Price (1980), Nitrous oxide solubility in water and seawater, *Mar. Chem.*, *8*(4), 347–359, doi:10.1016/0304-4203(80)90024-9.

Westley, M. B., H. Yamagishi, B. N. Popp, and N. Yoshida (2006), Nitrous oxide cycling in the Black Sea inferred from stable isotope and isotopomer distributions, *Deep Sea Res. Part II Top. Stud. Oceanogr.*, *53*(17–19), 1802–1816, doi:10.1016/j.dsr2.2006.03.012.

de Wilde, H. P., and M. J. de Bie (2000), Nitrous oxide in the Schelde estuary: production by nitrification and emission to the atmosphere, *Mar. Chem.*, *69*(3–4), 203–216, doi:10.1016/S0304-4203(99)00106-1.

Yamagishi, H., M. B. Westley, B. N. Popp, S. Toyoda, N. Yoshida, S. Watanabe, K. Koba, and Y. Yamanaka (2007), Role of nitrification and denitrification on the nitrous oxide cycle in the eastern tropical North Pacific and Gulf of California, *J. Geophys. Res. Biogeosciences*, *112*(G2), G02015, doi:10.1029/2006JG000227.

Yoshida, N., H. Morimoto, M. Hirano, I. Koike, S. Matsuo, E. Wada, T. Saino, and A. Hattori (1989), Nitrification rates and 15N abundances of N_2O and NO_3^- in the western North Pacific, *Nature*, *342*(6252), 895–897, doi:10.1038/342895a0.

Yoshinari, T. (1976), Nitrous oxide in the sea, *Mar. Chem.*, *4*(2), 189–202, doi:10.1016/0304-4203(76)90007-4.

Zamora, L. M., and A. Oschlies (2014), Surface nitrification: A major uncertainty in marine N_2O emissions, *Geophys. Res. Lett.*, *41*(12), 2014GL060556, doi:10.1002/2014GL060556.

Zamora, L. M., A. Oschlies, H. W. Bange, K. B. Huebert, J. D. Craig, A. Kock, and C. R. Löscher (2012), Nitrous oxide dynamics in low oxygen regions of the Pacific: insights from the MEMENTO database, *Biogeosciences*, *9*(12), 5007–5022, doi:10.5194/bg-9-5007-2012.

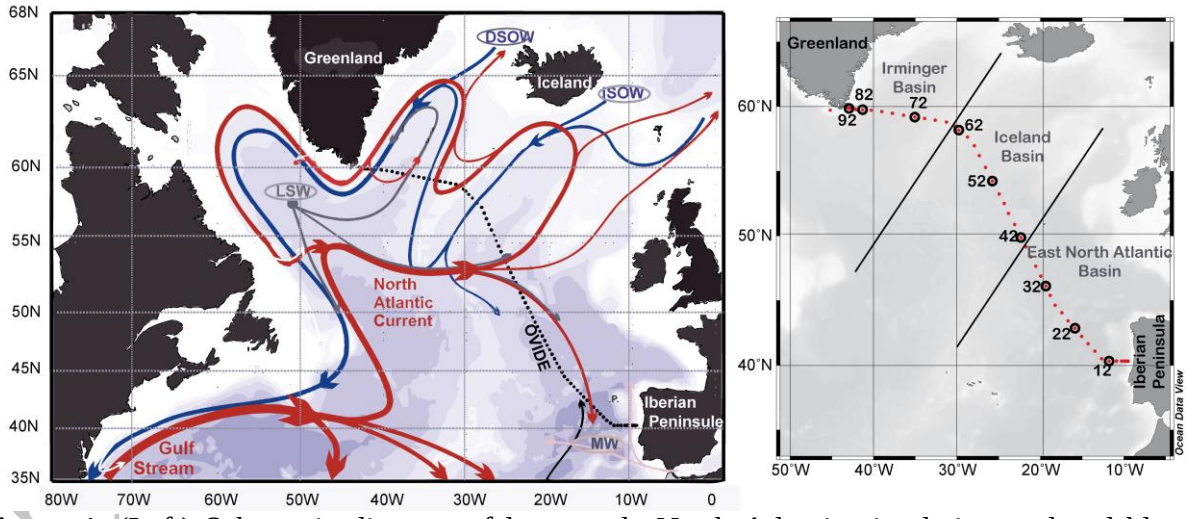

Figure 1. (Left) Schematic diagram of large-scale North Atlantic circulation, red and blue lines showing upper and deeper layers, respectively; isobaths are shown as blue shadows. Abbreviations of main water masses: Denmark Strait Overflow Water (DSOW), Iceland–Scotland Overflow Water (ISOW), Labrador Sea Water (LSW) and Mediterranean Water (MW). Stations of the 2012 OVIDE cruise are shown by black dots. (Right) Hydrographic stations (red points) of the 2012 OVIDE cruise. Black-lined points correspond to the reference stations referred to in the figures throughout this paper. The two straight lines are the boundaries for Irminger Sea, ant the Iceland and eastern North Atlantic basins.

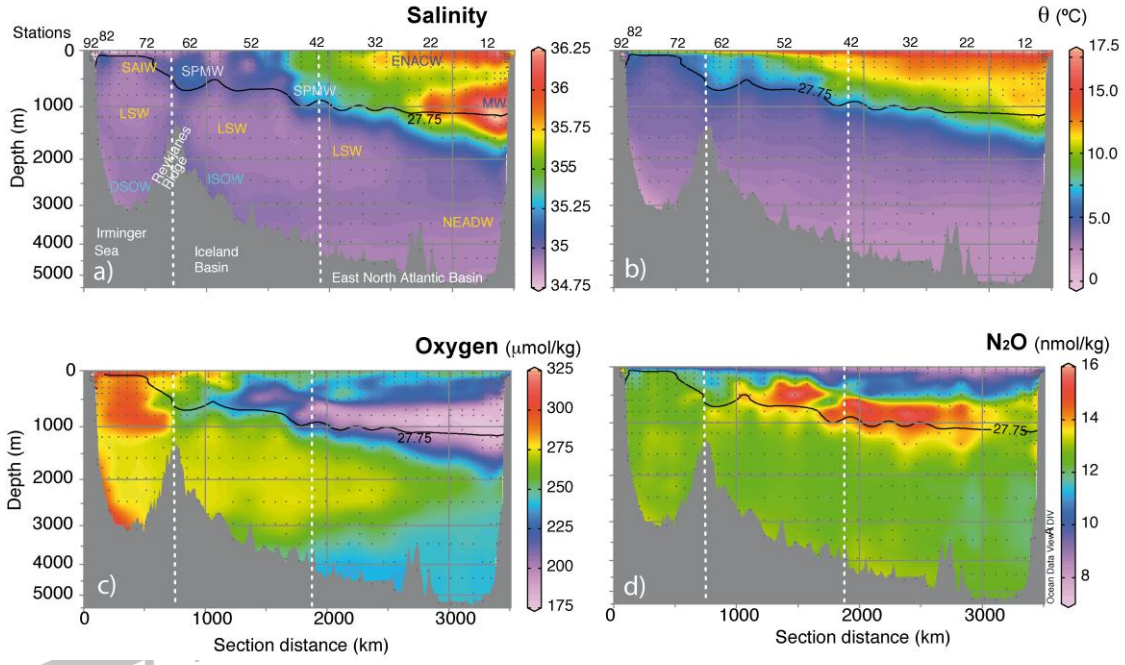

Figure 2. Distribution of (a) salinity, (b) potential temperature (θ), (c) dissolved oxygen and (d) N_2O along the OVIDE section in 2012. ENACW, eastern North Atlantic Central Water; ISOW, Iceland–Scotland Overflow Water; DSOW, Denmark Strait Overflow Water; SAIW, Subarctic Intermediate Water; SPMW, Subpolar Mode Water; MW, Mediterranean Water; LSW, Labrador Sea Water; NEADW, North-East Atlantic Deep Water. Dashed white lines delimit the boundaries of the Irminger Sea, the Iceland Basin and the eastern North Atlantic Basin, while the black line is the neutral density delimiting the upper and lower limbs of the AMOC (γ_n = 27.75). The numbers on the upper horizontal axis refer to the stations shown in Figure 1b.

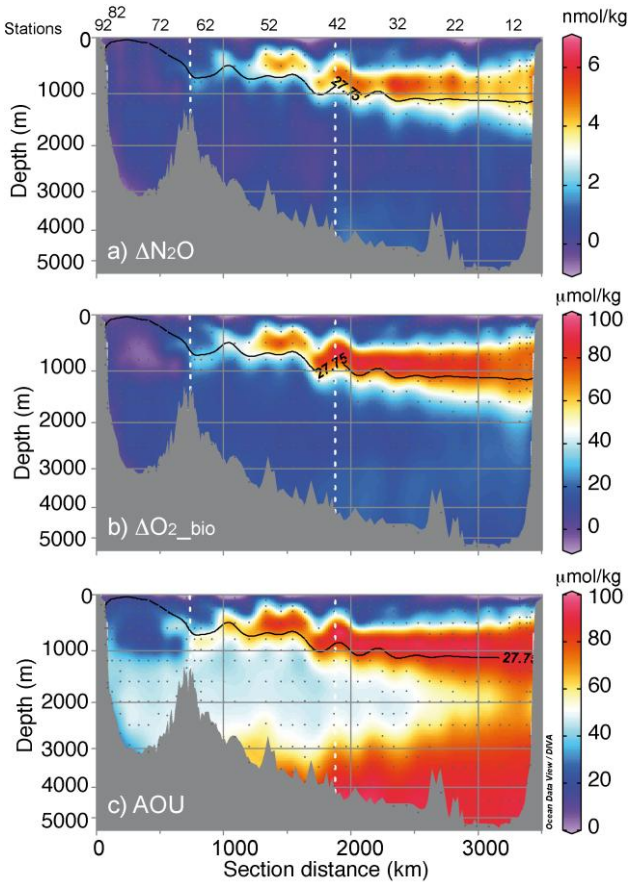

Figure 3. Distribution of (a) ΔN_2O, (b) ΔO_{2_bio} and (c) AOU along the OVIDE section. Dashed white lines delimit the boundaries for the Irminger Sea, the Iceland Basin and the eastern North Atlantic Basin. The black line represents the neutral density delimiting the upper and lower limbs of the AMOC (γ_n=27.75). The numbers on the upper horizontal axis refer to the stations shown in Figure 1b.

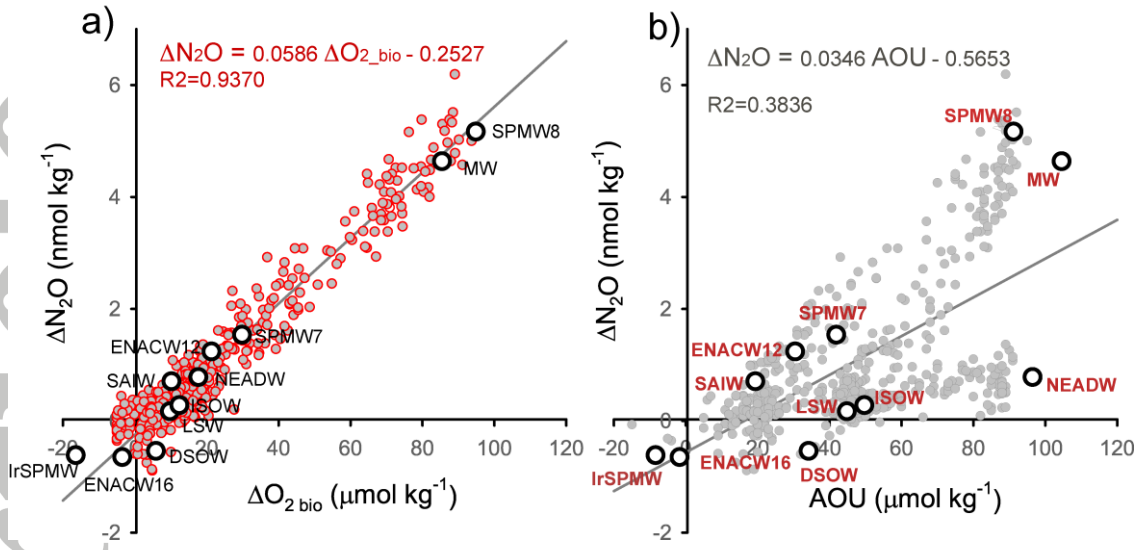

Figure 4. (a) ΔN_2O versus $\Delta O_{2\ bio}$ and (b) ΔN_2O versus AOU for the entire water column along the OVIDE section in 2012. Lineal fitting and the equation for the linear regression are shown. Averaged values for each water mass have been marked in white filled points: $ENACW_{16}$ and $ENACW_{12}$, Eastern North Atlantic Central Water of 16 and 12 ºC, respectively; MW, Mediterranean Water; SAIW, Subarctic Intermediate Water; $SPMW_7$ and $SPMW_8$: Subpolar Mode Water of 7 and 8 ºC, respectively; IrSPMW, Irminger Subpolar Mode Water; LSW, Labrador Sea Water; ISOW, Iceland–Scotland Overflow Water; DSOW, Denmark Strait Overflow Water; NEADW, North-East Atlantic Deep Water.

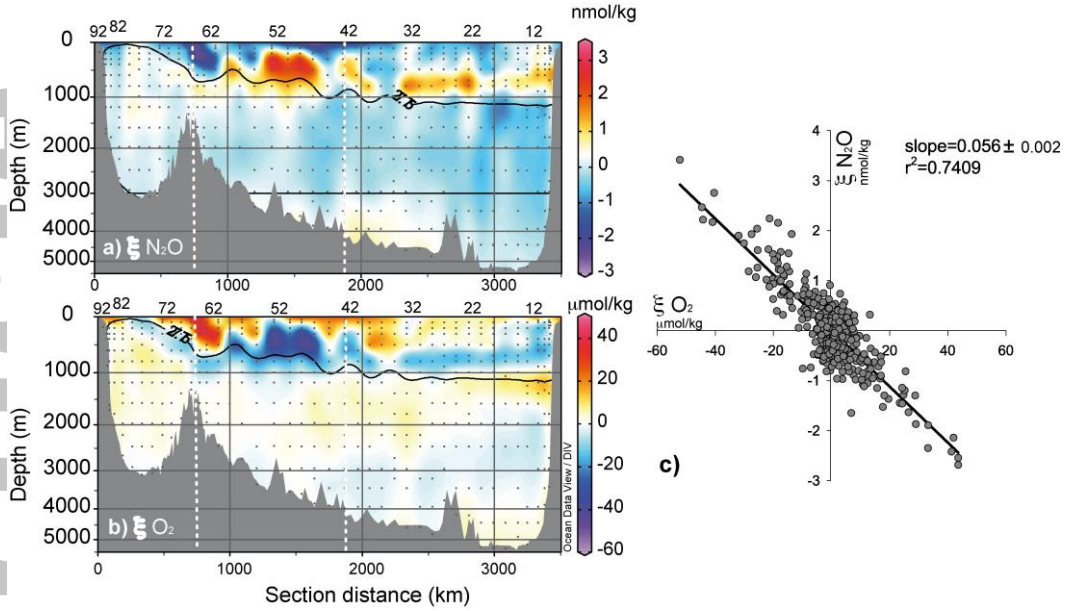

Figure 5. Distribution pattern of local remineralization: (a) ξN_2O and (b) ξO_2 along the OVIDE section in 2012 and (c) ξN_2O versus ξO_2, including linear fitting and equation for the linear regression. The neutral density delimiting the upper and lower limbs of the AMOC (γ_n = 27.75) is depicted in black. Dashed white lines delimit the Irminger Sea, the Iceland Basin and the Eastern North Atlantic Basin. The numbers on the upper horizontal axis refer to the stations shown in Figure 1b.

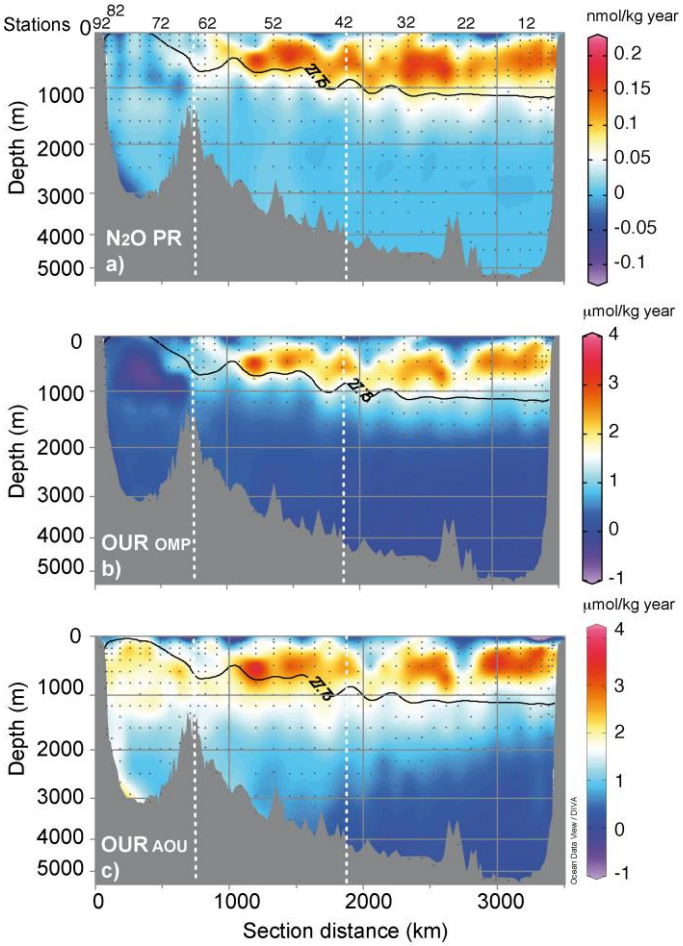

Figure 6. (a) Distribution of N_2O production rate (N_2O PR), (b) oxygen utilization rate (OUR) based on MLR from eOMP (OUR $_{OMP}$) and (c) OUR based on apparent oxygen utilization (OUR $_{AOU}$). The neutral density delimiting the upper and lower limbs of the AMOC (γ_n = 27.75) is depicted in black. Dashed white lines delimit the Irminger Sea, the Iceland Basin and the eastern North Atlantic Basin. The numbers on the upper horizontal axis refer to the stations shown in Figure 1b.

Table 1. Matrix of the thermohaline properties of the source water types (SWT)[a] considered in this study[b] and averaged N_2O and O_2 concentrations[c] in water masses obtained from equation (1)

SWT	θ [b] (ºC)	Salinity[b]	N_2O^{MT} [c] (nmol kg^{-1})	O_2^{MT} [c] (μmol kg^{-1})	ΔN_2O^{MT} [c] (nmol kg^{-1})	$\Delta O_{2\_bio}^{MT}$ [c] (μmol kg^{-1})
$ENACW_{16}$	16.00±0.13	36.20±0.02	7.88±0.34	244.73±5.20	-0.65	-3.48
$ENACW_{12}$	12.30±0.18	35.66±0.03	10.39±0.10	229.13±1.61	1.23	21.31
MW	11.7±0.2	36.500±0.011	13.28±0.25	155.95±3.84	4.64	85.43
SAIW	6.0±0.2	34.70±0.03	12.04±0.25	278.57±3.91	0.71	10.17
$SPMW_8$	8.00±0.11	35.230±0.016	15.52±0.21	195.04±3.18	5.17	94.82
$SPMW_7$	7.07±0.07	35.160±0.006	12.64±0.21	250.84±3.27	1.54	29.82
IrSPMW	5.00±0.02	35.014±0.013	12.00±0.29	316.53±4.53	-0.62	-16.46
LSW	3.00±0.19	34.87±0.02	12.64±0.10	277.14±1.53	0.17	9.75
ISOW	2.60±0.08	34.980±0.003	12.84±0.20	276.18±3.09	0.28	12.37
DSOW	1.30±0.06	34.905±0.006	13.28±0.25	302.65±10.38	-0.54	5.87
$NEADW_L$	1.98±0.03	34.895±0.003	12.33±0.14	234.39±2.11	0.78	17.68
r^{2} [d]			0.72	0.87	0.73	0.78
SD[d]			0.70	28.52	0.73	10.73

[a] $ENACW_{16}$ and $ENACW_{12}$, Eastern North Atlantic Central Water of 16 and 12 ºC, respectively; MW, Mediterranean Water; SAIW, Subarctic Intermediate Water; $SPMW_7$ and $SPMW_8$: Subpolar Mode Water of 7 and 8 ºC, respectively; IrSPMW, Irminger Subpolar Mode Water; LSW, Labrador Sea Water; ISOW, Iceland–Scotland Overflow Water; DSOW, Denmark Strait Overflow Water; $NEADW_L$, lower North-East Atlantic Deep Water.

[b] Preformed thermohaline properties of the SWTs used in the eOMP analysis (see supplementary information).

[c] Obtained by applying the least-squares regression of equation (1). The mixing type properties include an inventory of remineralization by the time they entered the OVIDE section.

[d] The r^2 and standard deviation (SD) correspond to the regression coefficient of observed A_j concentrations versus that obtained as the sum of the contributions by mixing of the individual types ($\sum_i^{11} X_{i,j}\, A_i^{MT}$).